NASA Technical Memorandum 84343

Flight Measurements of Hinged-Plate Wing-Spoiler Hinge Moments

Emmett B. Fry

September 1983

National Aeronautics and
Space Administration

NASA Technical Memorandum 84343

Flight Measurements of Hinged-Plate Wing-Spoiler Hinge Moments

Emmett B. Fry, Ames Research Center, Moffett Field, California

National Aeronautics and
Space Administration

Ames Research Center
Moffett Field, California 94035

NOMENCLATURE

$C_{D_{SP}}$	spoiler drag coefficient, drag force/$q_o S_{SP}$
$C_{h_{SP}}$	spoiler hinge moment coefficient, $M_{SP}/q_o \bar{c}_{SP} S_{SP}$
C_L	lift coefficient, lift force/$q_o S$
$\bar{c}_w$	wing mean aerodynamic chord
c_{SP}	spoiler mean aerodynamic chord
d_1	hydraulic actuator to torque tube lever arm
d_2	torque tube to spoiler lever arm
d_3	spoiler control horn lever arm
ESHP	equivalent shaft horsepower
F_1	force in hydraulic actuator
F_2	force in spoiler push-pull rod
KCAS	knots calibrated airspeed
KIAS	knots indicated airspeed
$K_{L.SP.}$	multiplying factor for lower spoiler
$K_{U.SP.}$	multiplying factor for upper spoiler
LLI	left lower inboard spoiler panel
LLO	left lower outboard spoiler panel
LUI	lower upper inboard spoiler panel
LUO	lower upper outboard spoiler panel
$M_{L.SP.}$	lower spoiler hinge moment
$M_{U.SP.}$	upper spoiler hinge moment
M_{TT}	torque tube hinge moment
q_o	dynamic pressure at sea level
RLI	right lower inboard spoiler panel
RLO	right lower outboard spoiler panel
RUI	right upper inboard spoiler panel

RUO	right upper outboard spoiler panel
S	airplane wing area
S_{SP}	spoiler panel area
SPPRS	spoiler hydraulic actuator differential pressure
STOL	short takeoff and landing
V_c	calibrated airspeed
W	airplane weight
α	angle between actuator arm and torque tube arm
β	angle between torque tube arm and spoiler push-pull rod
$\delta_{L.SP.}$	lower spoiler deflection angle
δ_{SP}	spoiler deflection angle
$\delta_{U.SP.}$	upper spoiler deflection angle
ϕ	angle between spoiler push-pull rod and spoiler control arm

SUMMARY

In-flight measurements were made of hinged-plate wing spoiler hinge moments. The twin turboprop airplane used in this study was modified by the addition of upper and lower wing-surface spoilers, and the spoiler-actuating hydraulic cylinders were instrumented to measure the forces required to extend the spoiler panels. Those measurements were converted to moment coefficient form, and are presented as a function of spoiler deployment angle.

The hinge-moment data were collected at three flight conditions: with flaps extended at approach speed; with flaps retracted at a low speed; and with flaps retracted at a high speed (C_L = 1.4, 1.0, and 0.5).

In general, the magnitude of measured spoiler hinge moments were lower than predicted. Furthermore, for upper surface spoilers with flaps extended, the hinge moments increased in a discontinuous manner between spoiler deflections $<10°$ and $>10°$.

INTRODUCTION

A DeHavilland DHC-6, Series 100 Twin Otter STOL transport (fig. 1), modified by the addition of a hinged-plate wing upper-surface spoiler/lower-surface dive brake

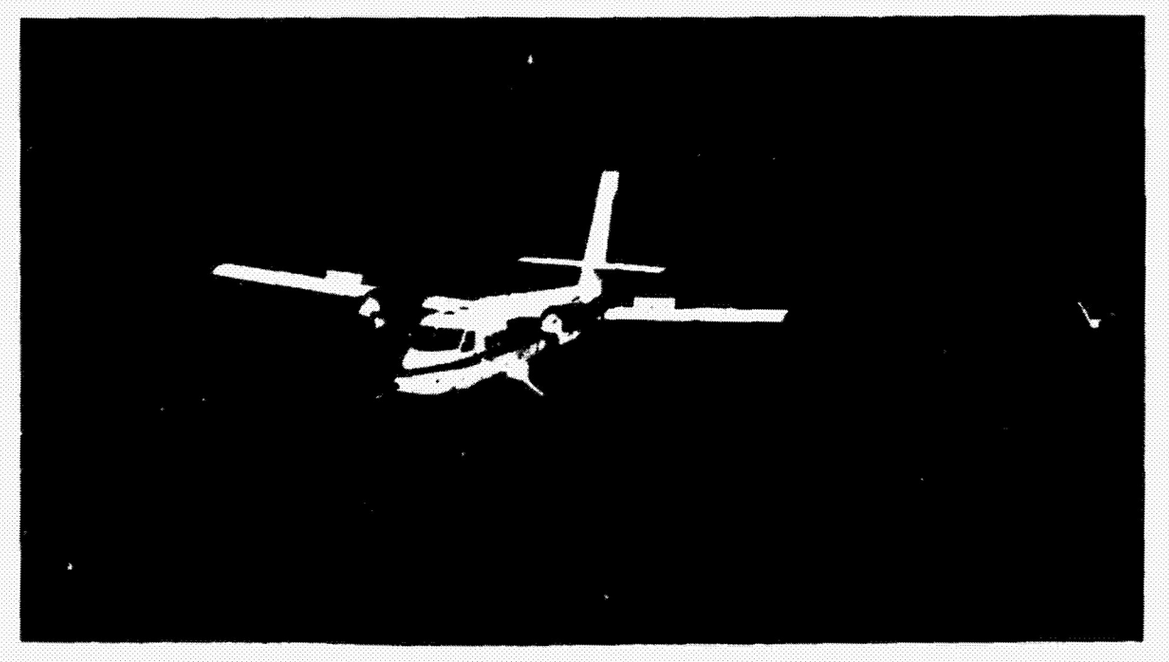

Figure 1.- Modified DHC Twin Otter with upper outboard glidepath spoilers extended.

system (hereafter referred to as "spoiler system"). The spoiler system is shown in figures 2 and 3, and its characteristics are given in table 1. This system has been evaluated in flight to determine the influence of spoiler controls on flying qualities for approach and landing for this category of airplane. The availability of a spoiler system on a fully instrumented airplane provided a rare opportunity to collect spoiler-hinge moment data in flight.

During the structural design phase of the Twin Otter spoiler system, a literature survey failed to reveal applicable hinge moment data. Although the literature did reveal some sophisticated theoretical spoiler aerodynamic prediction methods from which hinge moments could be calculated (ref. 1), the authors of those works invariably expressed low confidence in the validity of their calculations. Little experimental data from large scale wind-tunnel tests or flight tests exist to support the theoretical methods. During the DHC-6 flight research program, Ames Research Center was requested by industry to obtain spoiler-hinge moment data from the aircraft. With motivation provided by those requests and the scarcity of such data, the flight test program described here was developed.

The test methodology is described, and the hinge moment data that were obtained is presented. No attempt is made to provide correlation with theoretical methods, other than to compare this data with the predictions of hinge moment for this DHC-6 design installation.

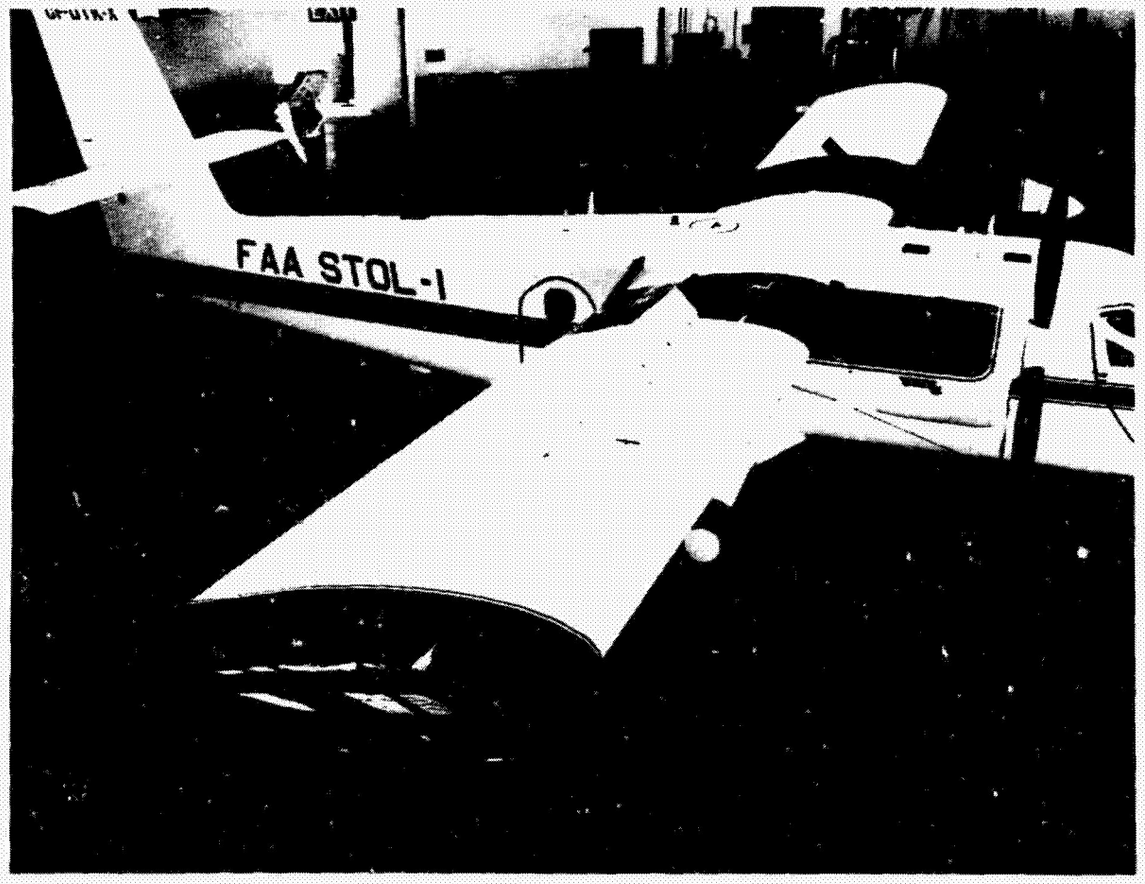

Figure 2.- Test airplane with inboard and outboard glidepath spoilers and right roll spoiler extended.

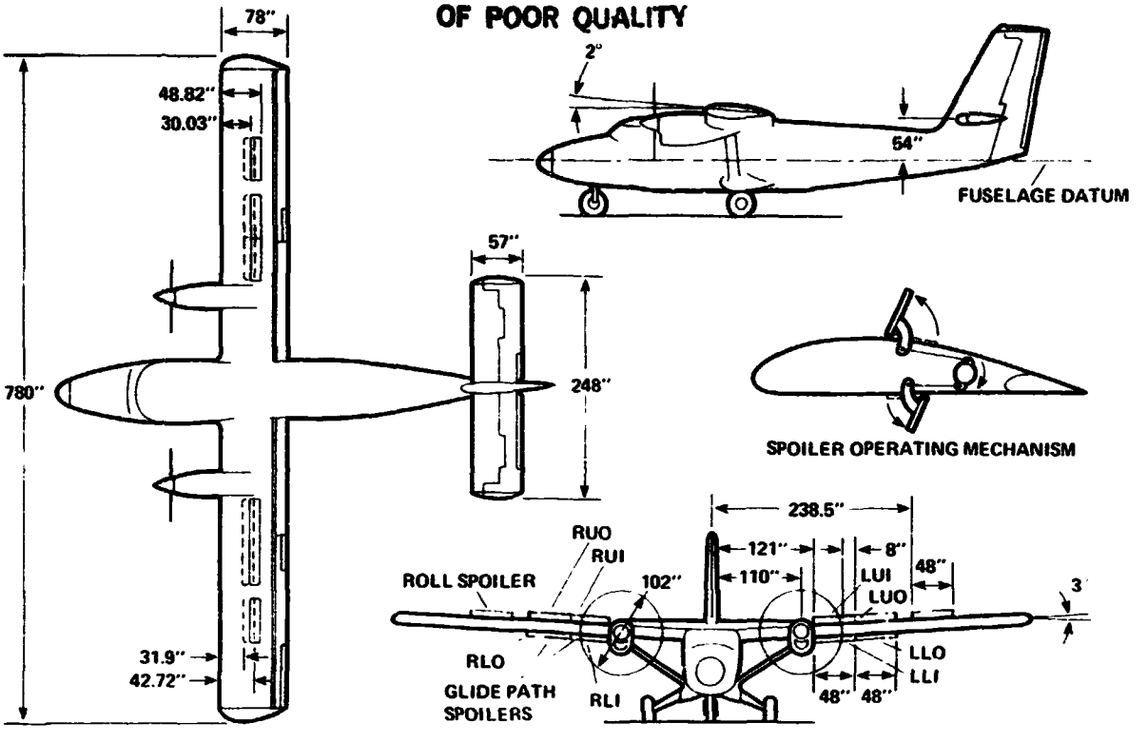

Figure 3.- Three view drawing of DHC-6 Twin Otter with wing spoiler modification.

TABLE 1.- SPOILER CHARACTERISTICS

Characteristic	Upper surface panel	Lower surface panel
Span	1.22 m (4.0 ft)	1.22 m (4.0 ft)
Chord	0.305 m (1.0 ft)	0.229 m (0.75 ft)
Maximum angle	51°	51°
Panel area	0.372 m^2 (4.0 ft^2)	0.279 m^2 (3.0 ft^2)
Total glidepath panels	4	4
Total roll panels	2	2
Location of hinge line aft of the wing leading edge	0.763 m (2.50 ft), 0.385 $\bar{c}$	1.085 m (3.56 ft), 0.548 $\bar{c}$

DESCRIPTION OF FLIGHT TEST

Test Airplane

The DeHavilland DHC-6, series 100 Twin Otter airplane is shown in flight (fig. 1) with the upper outboard spoiler panels (RUO) and left-upper outboard spoiler panel (LUO) deployed. Figure 2 shows the airplane on the ground with all spoiler panels

fully deployed. The spoiler modification, the essential dimensions, and the identification of the spoiler panels for the airplane is shown (fig. 3). A sketch of the spoiler operating mechanism is included in the inset. The basic airplane general characteristics are listed in table 2.

TABLE 2.- TEST AIRPLANE CHARACTERISTICS

Weight - maximum takeoff	5,252 kg (11,579 lb)
- maximum landing	4,990 kg (11,000 lb)
Engines	(2)PT6a-20A (579 ESHP)
Flaps	Full span, double slotted
Wing loading, W/S	127.92 kg/m^2 (26.2 lb/ft^2)
Power loading	3.05 kg/ESHP (10.0 lb/ESHP)
Wing span	19.81 m (65 ft)
Wing area	39.02 m^2 (420 ft^2)
Mean aerodynamic chord	1.98 m (6.5 ft)
Aspect ratio	10.0
Airfoil section	DHC L-18
Airfoil thickness ratio	17%
Maximum lift coefficient	2.6
Stall speed, V_{so}	56 KCAS
Approach speed, 1.3 V_{so}	73 KCAS

Spoiler System

The Twin Otter wing-spoiler modification consisted of two upper- and two lower-surface hinged-plate panels on each wing for glidepath control. For roll control, an upper and lower outboard panel identical to those for glidepath control was provided outboard of the glidepath panels on each wing.

These spoilers are similar to those in current use on sailplanes manufactured in the United States. The upper and lower panels are linked to a common torque tube (fig. 3 inset).

All spoiler panels were located at approximately the 50% wing chord position. The exact chordwise and spanwise location of the spoiler panels and other geometric details can be seen (figs. 3-5). Principal characteristics are given in table 1.

To reduce the aerodynamic wake effects, the spoiler panels were vented by slots located near the hinge line (ref. 2). No venting path existed between the lower and upper panels, and it was not feasible to provide one because of the interference of the wing structure.

The particular spoiler panels which were used to determine hinge moments were the outboard upper and lower spoiler set identified as right-upper outboard spoiler panel (RUO), left-upper outboard spoiler panel (LUO), right-lower outboard spoiler panel (RLO), and left-lower outboard spoiler panel (LLO) (fig. 3). The inboard edges of these panels are located about 8 in. outboard of the propeller arc, and are thus likely to avoid the influence of the propeller wake. The area of the upper panels was 4.0 ft^2, and the area of the lower panels was 0.28 m^2 (3.0 ft^2). Maximum deflection was approximately 51° for both upper and lower surfaces.

Flight Plan of Test

Data for upper and lower spoilers were recorded during steady-state trimmed flight at each of three conditions: 75 knots indicated airspeed, knots (KIAS) with maximum flaps, and 90 KIAS and 125 KIAS with zero flaps. This corresponds to C_L = 1.4, 1.0, and 0.5, respectively. At each speed, the spoilers were sequenced to full deployment in 6 steps, allowing 1 min of data taking at each spoiler opening.

Engine power was set to the value required for level flight with spoilers closed; therefore altitude was lost as the spoilers were progressively opened for each data point. After data were taken for each speed and spoiler configuration at full spoiler deflection, an additional data point was taken with idle thrust to assess the effects of propeller slipstream on the hinge moments.

Since the upper and lower spoiler panels are both connected to a common torque tube (fig. 3), the ones to be removed had to be alternately disconnected and reconnected via the appropriate push-pull rods. When the upper panels were deactivated by removing their push-pull rods, the panels were retained on the airplane by bolting their trailing edges to the wing skin. With the lower panels, the entire panels, hinge pins, and push-pull rod assemblies were removed from the airplane.

Data System

The data acquisition and recording system used in the Twin Otter airplane had a maximum capability of 180 channels of information (ref. 3). For these tests, however, only 30 data channels were required.

The primary source of data telemetered in real time to the ground facility, and displayed by alphanumeric printouts on an electrostatic printer (table 3) and also by time-history traces on strip-chart recorders. These data sources were supported by airborne and ground-generated magnetic tape recordings.

Instrumentation and Data Reduction

Cockpit instrumentation consisted of Twin Otter conventional blind flying panel plus the Electronic Attitude Director Indicator and the Electronic Horizontal Situation Indicator (ref. 1). This instrumentation was only important to these tests in that the digital airspeed readout and the autopilot speed-hold mode simplified the piloting task of stabilizing airspeed while deploying the spoilers. Spoiler position was displayed by micrometer edge gauges mounted on the glareshield.

To measure the spoiler hinge moments, strain gauge differential pressure sensors were installed across the two sides of the double action pistons of the spoilers' hydraulic actuators. Hinge moments were then calculated from the force applied by the actuator to the spoilers through the control linkage geometry. The upper- and lower-spoiler actuating systems are shown in figures 4 and 5.

Since the spoiler actuating system results in a nonlinear gearing, the mechanical advantage of the system was determined as a function of spoiler position. The gearing that resulted from the hydraulic actuator was then combined with the mechanical gearing to form a multiplying factor — at a given spoiler deflection — which determines spoiler hinge moment when multiplied by hydraulic actuator differential pressure

TABLE 3.- REAL TIME TELEMETRY PRINTOUT

GROUND TIME : DDD-HH-MM-SEC 054-19-49-25.069 | AIRCRAFT TIME : DDD-HH-MM-SEC 054-19-49-25.069 | DELTA TIME (SEC'S) 0.000 | PP | 85

*(001) TTRX # FEET	*(002) TTRY # FEET	*(003) TTRZ # FEET	*(004) MTRX # FEET	*(005) MTRY # FEET
*(006) MTRZ # FEET	(007) THETA #DEG	(008) PHI #DEG	(009) VCAIRF#FT/SEC	(010) THTDOT#DEGSEC
(011) RALTF #FT	(012) PHIDOT#DEGSEC	(013) VTAIRF#FT/SEC	(014) FPAAIR#DEG	(015) YEPR #FT
(016) GAMMAI#DEG	(017) HERRG #FT	(018) LIDRUM#RADSEC	(019) ELVPOS#DEG	(020) LODRUM#DEG
(021) RIDRUM#DEG	(022) ACCZB # G	(023) RODRUM#DEG	(024) XRN #FT	(025) TQPRSL#PSI
(026) DELFLP#DEG	(027) PSIA #DEG	(028) TQPRSR#PSI	(029) PSIDOT#DEGSEC	(030) RUDPOS#DEG
(031) TOTTMP#DEG.C	(032) AILPS #DEG	(033) LPWRLV#IN	(034) LRPM #	(035) RRPM #%
(036) ALPHAS#G	(037) BETAS #DEG	(038) TRIMPS#	(039) RSPPRS#RAWLPS	(040) RSPPRS#PSI/CT
(041) LSPPRS#RAWRPS	(042) LSPPRS#PSI/CT	(043) USAF1 #RAWUSA	(044) USAF1 #KNOTS	

054-19-49-25.069

(001) 3.593872E 04	(002) -1.279968E 04	(003) -4733.994	(004) 3.595487E 04	(005) -1.278397E 04
(006) -4744.943	(007) -1.06195	(008) 3.95594	(009) 209.90	(010) 7.7840E-02
(011) 491.74	(012) -0.56155	(013) 222.90	(014) -5.32783	(015) -36.000
(016) -5.50996	(017) 319.50	(018) 51.364	(019) 1.29249	(020) 1.23506
(021) 51.108	(022) 1.1000E-02	(023) -0.48678	(024) 3.6392E 04	(025) 36.350
(026) 0.44734	(027) -93.373	(028) 39.360	(029) -4.1699E-02	(030) 9.91419
(031) -0.60591	(032) 0.40120	(033) 1.58104	(034) 77.034	(035) 75.728
(036) 3.73420	(037) -1.07319	(038) -6.32499	(039) 1023.0	(040) 1237.3
(041) 1023.0	(042) 1234.3	(043) 494.00	(044) 94.411	

054-19-49-26.581

(001) 3.596268E 04	(002) -1.309998E 04	(003) -4703.636	(004) 3.597562E 04	(005) -1.308684E 04
(006) -4719.260	(007) -1.15647	(008) 4.03378	(009) 209.90	(010) 0.13899
(011) 491.74	(012) 0.13899	(013) 222.80	(014) -5.43742	(015) -36.000
(016) -5.62949	(017) 319.50	(018) 51.365	(019) 1.21500	(020) 1.36421
(021) 51.117	(022) 2.1000E-02	(023) -0.80957	(024) 3.6544E 04	(025) 36.350
(026) 0.43956	(027) -93.461	(028) 39.360	(029) -2.2239E-02	(030) 9.91419
(031) -0.75247	(032) 0.13220	(033) 1.55484	(034) 76.966	(035) 75.794
(036) 4.00269	(037) -0.68960	(038) -6.37559	(039) 1023.0	(040) 1237.3
(041) 1023.0	(042) 1234.3	(043) 496.00	(044) 94.980	

054-19-49-27.589

(001) 3.597623E 04	(002) -1.330193E 04	(003) -4681.153	(004) 3.599217E 04	(005) -1.328723E 04
(006) -4697.965	(007) -1.19262	(008) 3.93648	(009) 209.30	(010) 0.00000
(011) 491.74	(012) 0.57823	(013) 222.10	(014) -5.58958	(015) -36.000
(016) -5.74347	(017) 319.50	(018) 51.393	(019) 1.21500	(020) 1.36421
(021) 51.091	(022) 6.0000E-03	(023) -0.48678	(024) 3.6540E 04	(025) 36.400
(026) 0.43955	(027) -93.473	(028) 39.400	(029) -0.30302	(030) 9.86439
(031) -0.75247	(032) 0.13220	(033) 1.58759	(034) 76.796	(035) 75.826
(036) 4.11009	(037) -1.01840	(038) -6.08679	(039) 1023.0	(040) 1237.3
(041) 1023.0	(042) 1234.3	(043) 496.00	(044) 94.980	

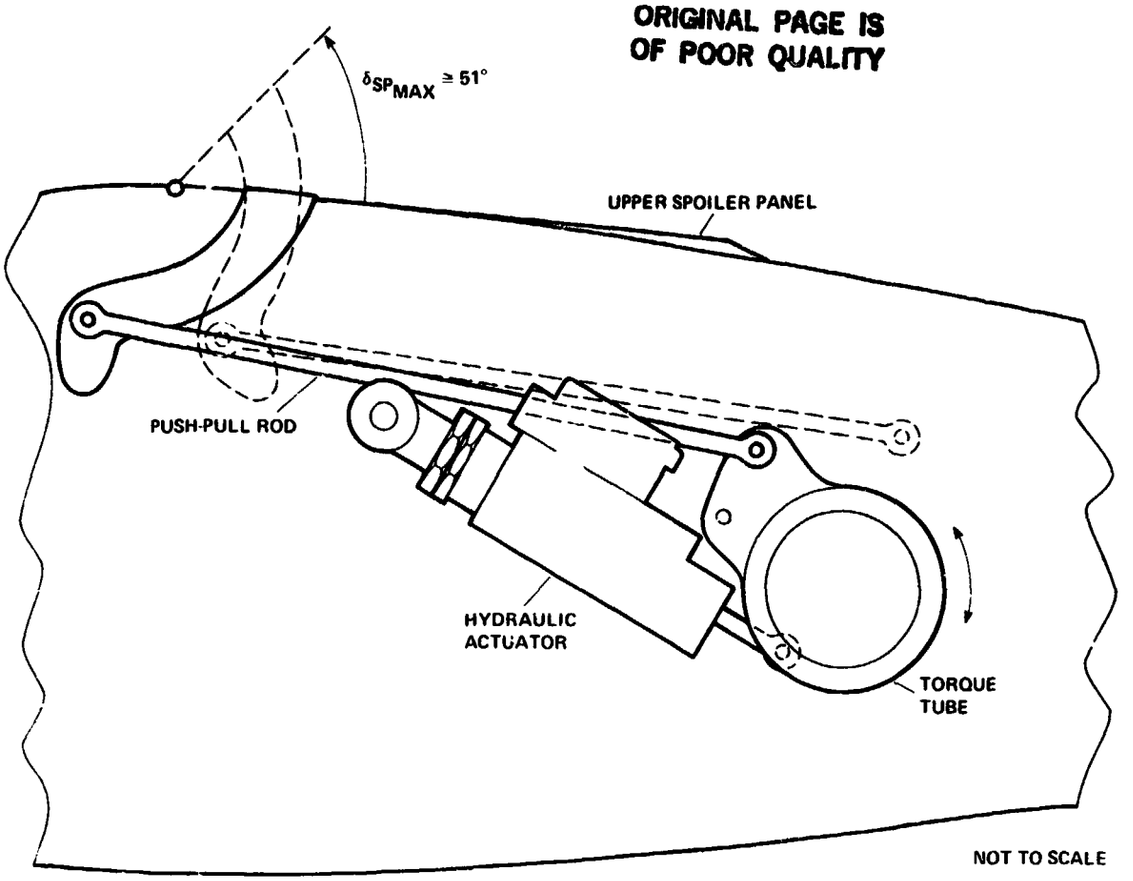

Figure 4.- Upper spoiler actuating system.

(SPPRS). The multiplying factors for upper and lower spoiler systems are shown in figure 6. The method of deriving the multiplying factors is given in the appendix.

Data Processing

The hinge moment calculations were performed manually from the alphanumeric printouts (table 3). These printouts consisted of blocks of discrete data bursts in real time. The pertinent mnemonics are given in the nomenclature. Each point shown in the hinge moment plots was computed from a burst of real time data of approximately 45 sec. Wild points were discarded and were defined as greater than twice, or less than one-half of the mean values. One sigma variations were computed and plotted for each point.

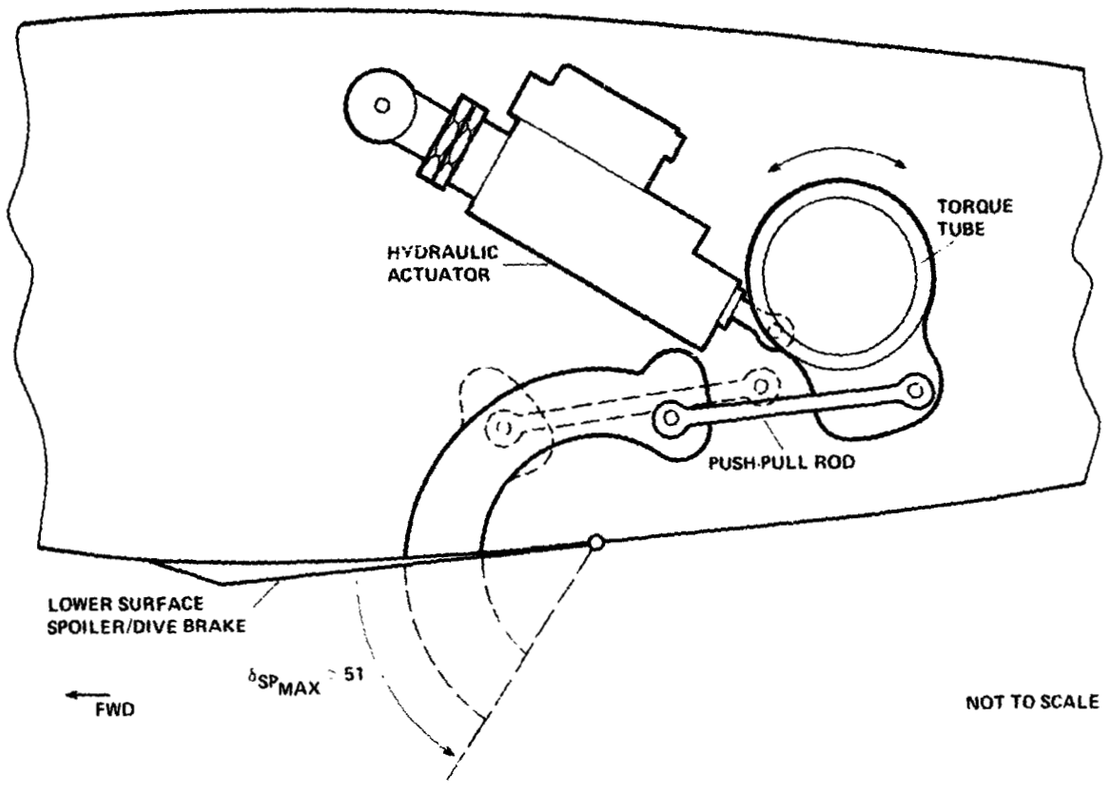

Figure 5.- Lower spoiler actuating system.

RESULTS AND DISCUSSION

Upper Surface Spoilers

Upper-surface spoiler-hinge moments are plotted as a function of spoiler deflection in figures 7a, b, and c. The upper and lower boundaries of the hinge moment coefficient envelope are defined by one-sigma values from the extreme data points as indicated on the plots.

A dashed line (fig. 7) for the hinge moment indicates the resulting spoiler drag coefficient of $C_{D_{SP}} = 2.0$ (refs. 4 and 5) acting at the centroid of the exposed panel area. This estimate of hinge moment was made to establish a lower limit for the structural design requirements.

For small values of spoiler deflection — up to 10° for the 75-knot case, and 20° to 25° for the 90-knot and 125-knot cases — the hinge moments were negative. Thus, without a closing hinge moment applied, the spoilers would have free-floated to those angles.

The most surprising revelation of these data can be seen in the 75-knot case (fig. 7a), which was the only flapped configuration tested. A sharp discontinuity can

be seen in the data at about 10° deflection. At that point, as the spoilers were slowly deployed, the airflow aft of the spoiler panel reattached after having been separated for lower angles of deployment.

The airflow around the spoilers can be visualized by observing the tuft photographs in figure 8. With spoilers closed (fig. 8a) the flow is attached, as would be expected. With the spoilers open approximately 10° (fig. 8b), the flow between the spoiler and the flap is separated, with some reverse flow indicated. With spoilers fully open (fig. 8c), the flow has reattached and was observed to reattach at approximately 15° spoiler deflection. It is possible that this flow reattachment is coincidental with the discontinuity in the hinge-moment data, although no specific testing was done to make this determination.

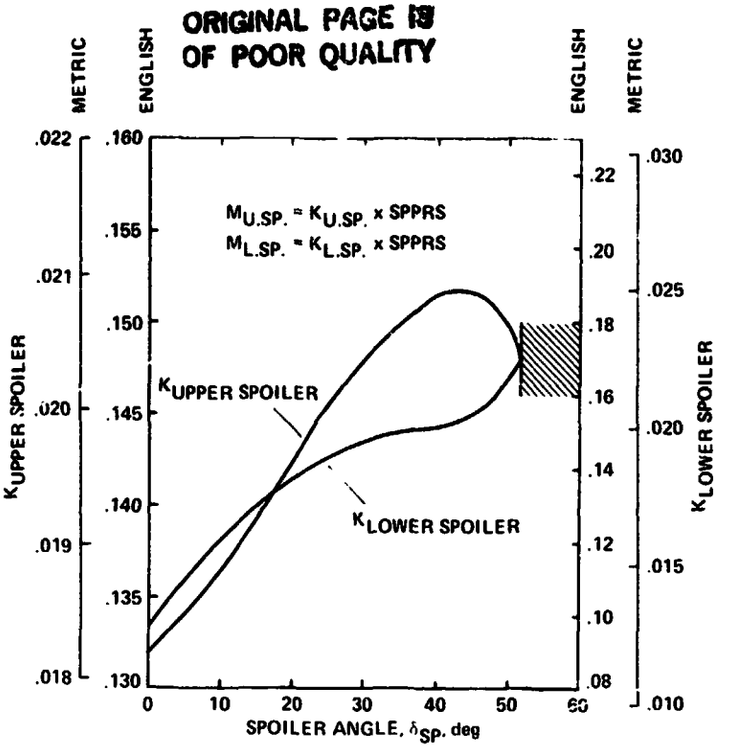

Figure 6.- Upper and lower spoiler multiplying factors to account for mechanical and hydraulic gearing.

The 90-knot and 125-knot zero flap configurations (figs. 7b-c), indicate a continuous variation of hinge moment coefficient with respect to spoiler angle. Observations of the tufts during flight indicated that flow separation occurred immediately as the spoilers were opened, and, unlike the 75-knot, 40°-flap configuration, the flow remained separated aft of the spoilers for all angles of deployment.

The only characteristic of the 90-knot data which might be considered anomalous is the negative slope of C_h vs δ_{SP} for the first few degrees of deployment.

The 90-knot and 125-knot data had a very small dispersion of standard deviation compared with the 75-knot case. The implication is that the flow was less turbulent, although separated, aft of the spoiler panels for the zero flap configurations that it was for the 40°-flap case.

Figure 3 indicates a 5-in. lateral separation between the propeller arc and the inboard edge of the active spoiler panel. Since it appeared possible for the propeller slipstream to effect the hinge moment measurement, the data point at maximum spoiler deflection was repeated with idle thrust.

Idle thrust data was then compared with power-on data (figs. 8a and 8c). The idle data, e.g., the flagged points (slightly lower value than the power points) were separated by less than one sigma variation than the powered points were. Therefore, propeller slipstream did not seem to have a significant influence on the hinge moment.

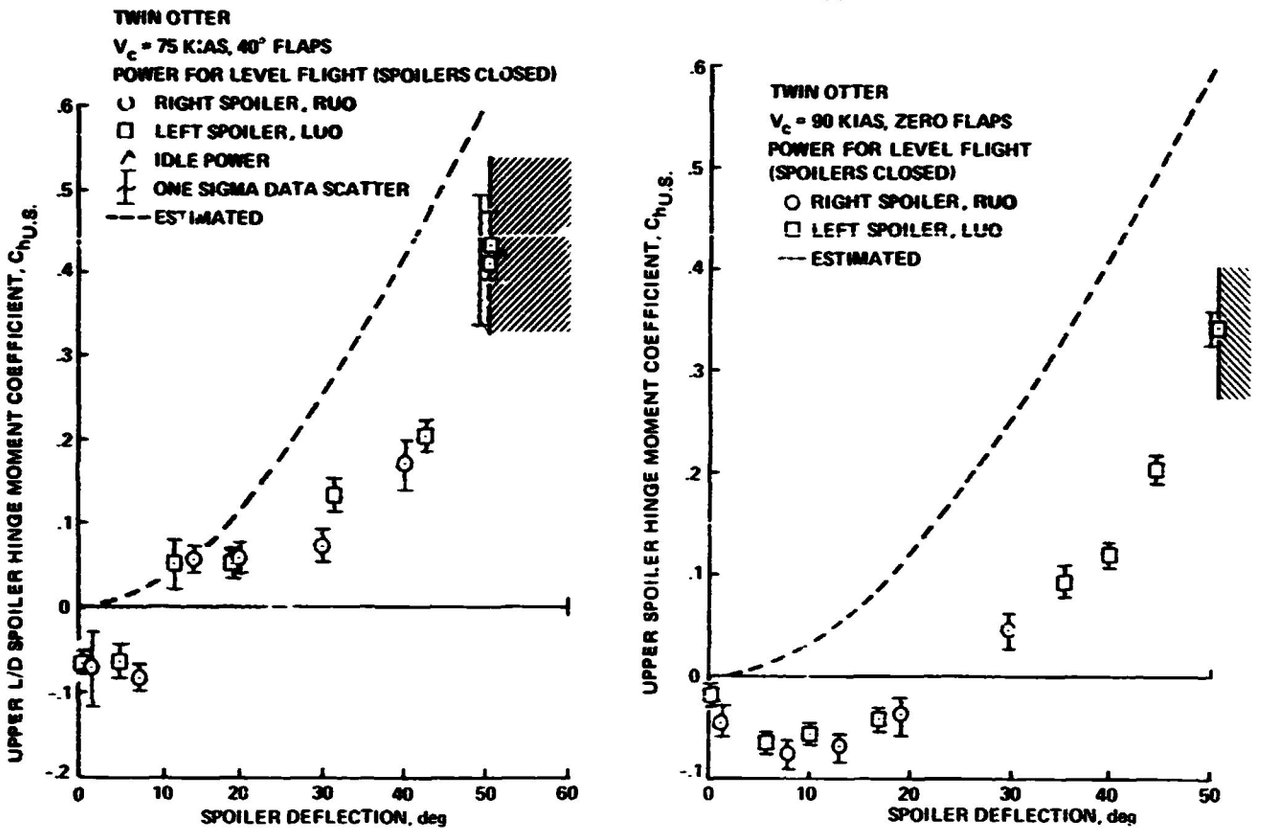

(a) 75 KIAS.

(b) 90 KIAS.

Figure 7.- Upper spoiler hinge moment coefficient.

Lower Surface Spoilers

Hinge-moment coefficient data for the lower surface spoilers indicate a relatively constant value, almost independent of spoiler deflection angle, for all conditions tested (fig. 9). As the spoilers were deployed, the hinge moment coefficient quickly built up to a value of $C_h \cong -0.1$, and maintained that value until $\delta_{SF} \cong 40°$ when the moments decreased with further deployment.

No flow visualization techniques were attempted to illustrate airflow patterns on the lower wing surface.

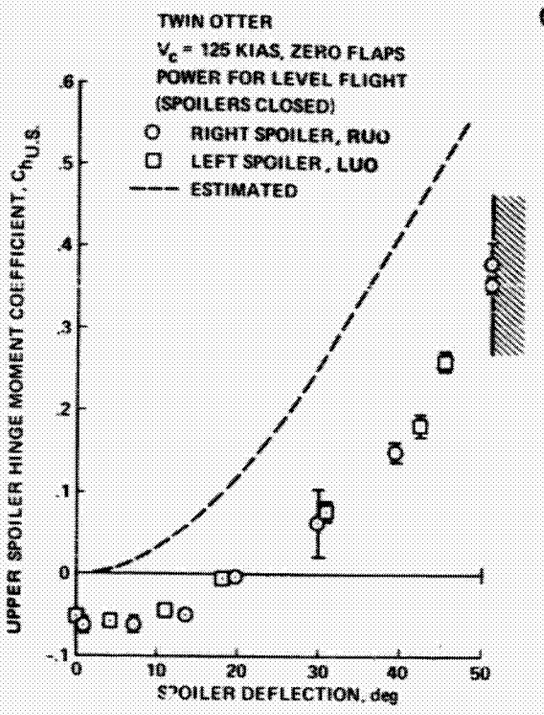

(c) 125 KIAS.

Figure 7.- Concluded.

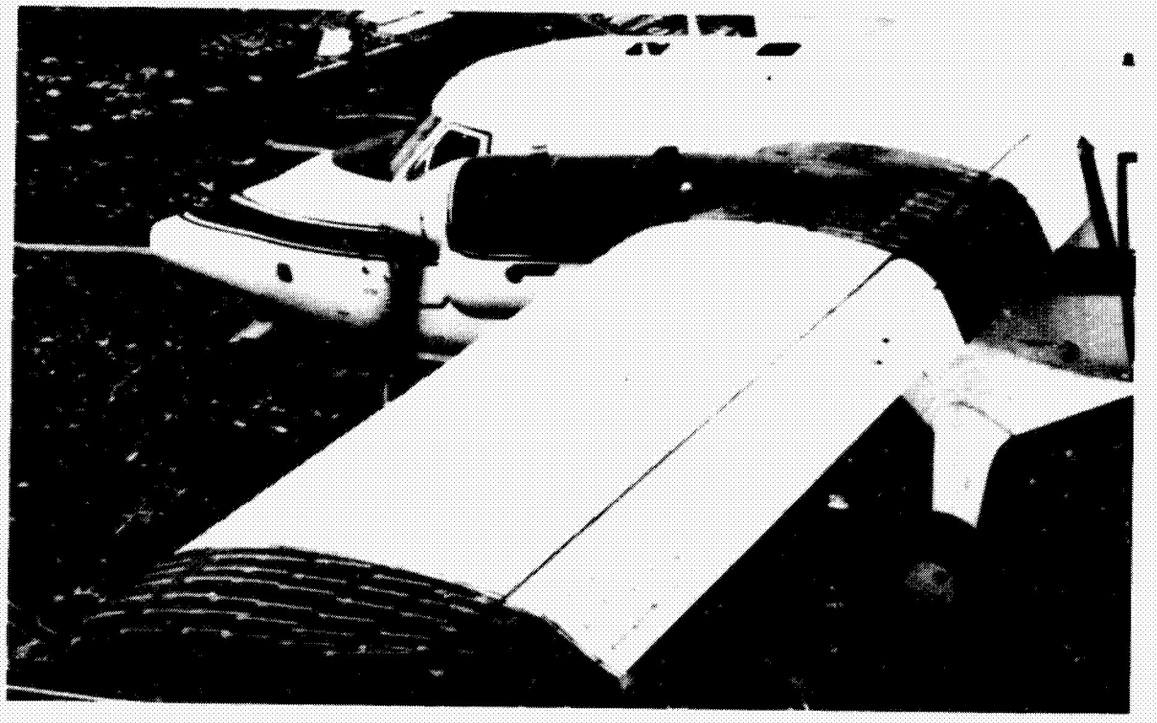

(a) Spoilers closed.

Figure 8.- Maximum flaps, 75 KIAS.

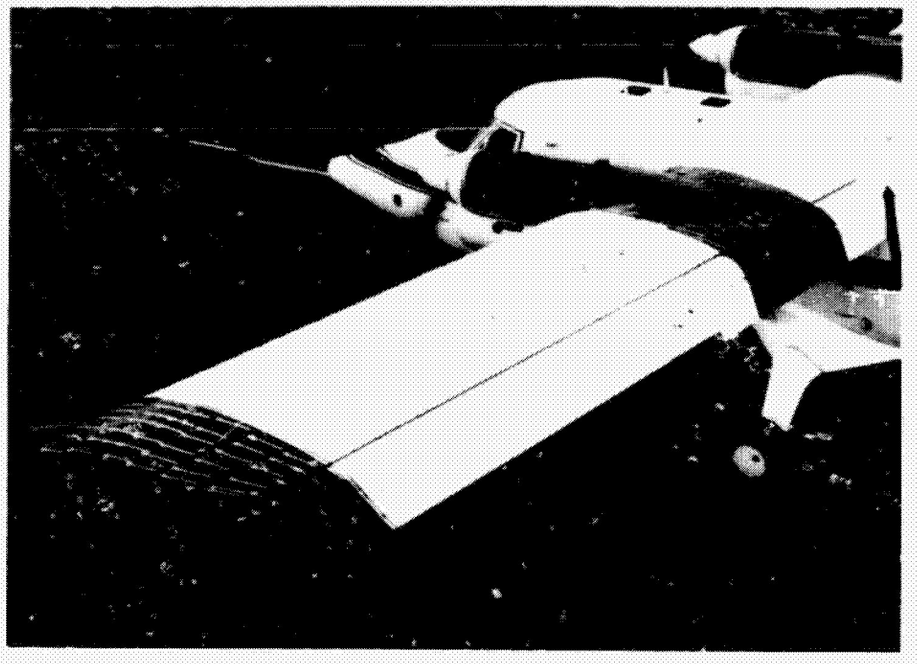

(b) LUO spoiler > 10°.

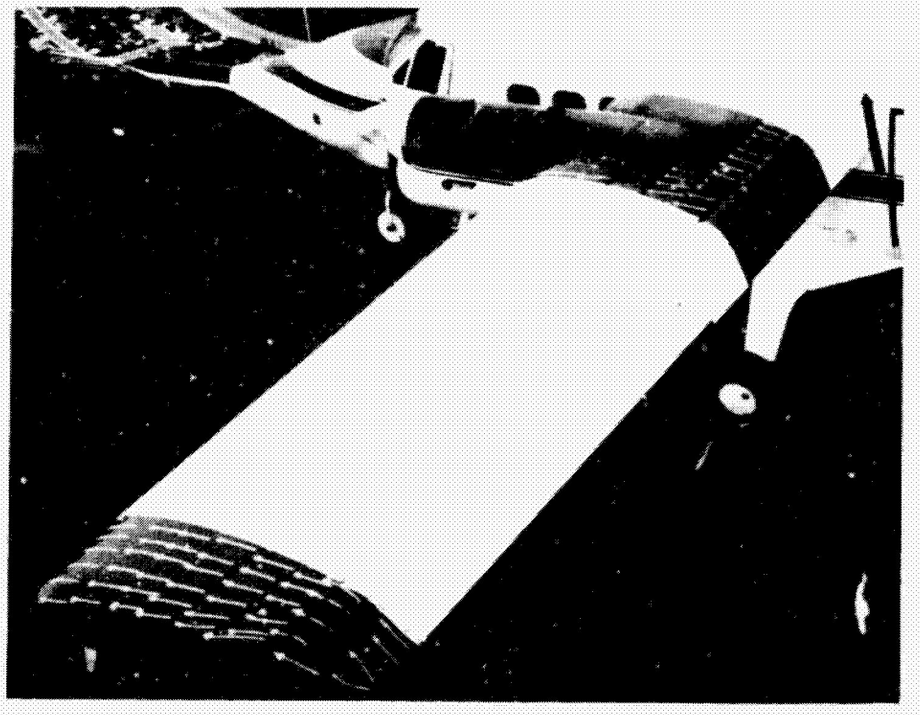

(c) LUO spoiler ≅ 51°.

Figure 8.- Concluded.

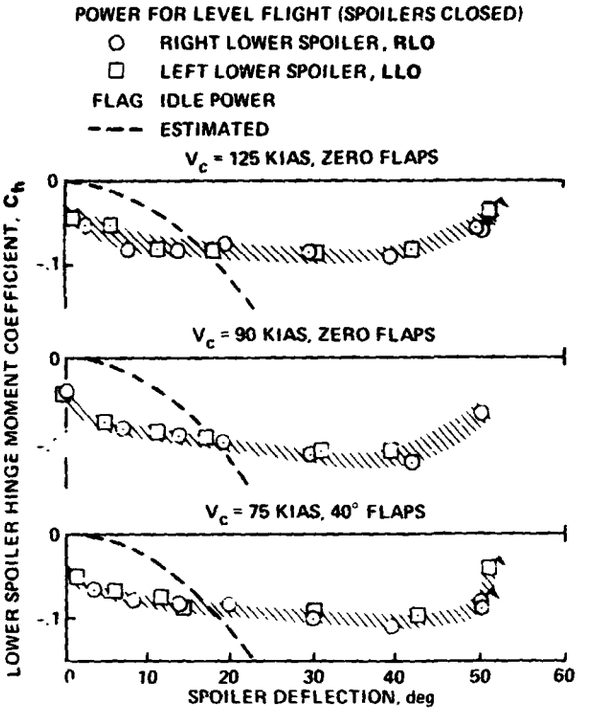

Figure 9.- Lower spoiler hinge moment coefficient.

CONCLUSIONS

In-flight measurements were made to determine hinge moment coefficients of upper and lower wing surface hinged-plate spoilers installed on a DHC-6 Twin Otter turboprop STOL transport.

In general, the magnitude of the hinge moments measured in flight were lower than predicted. Furthermore, for upper surface spoilers with the maximum flap deflection, a significant discontinuity existed for spoiler deflections <10° and >10°. The reason for the discontinuity cannot be established; however, it was observed to coincide with flow reattachment aft of the spoiler panel for spoiler deflections exceeding 10°.

APPENDIX

The procedure used to determine the mechanical gearing for both upper and lower spoiler-control linkage systems is described. The interplay of the control lever geometries results in a nonlinear relationship between the input torque-tube moment and the output spoiler-hinge moment. A trigonometric expression can be derived by determining sine values for three lever angles from a graph and by substituting into the expression. The gear ratio, or multiplying factor, can then be determined for any spoiler deflection angle.

In addition, the hydraulic advantage, or gearing is calculated as a factor to be multiplied by differential hydraulic pressure (SPPRS) to determine input force to the control linkage systems. This multiplying factor is the same for upper and lower spoilers since the same actuator is used for both systems.

Upper Spoiler Mechanical and Hydraulic Gearing

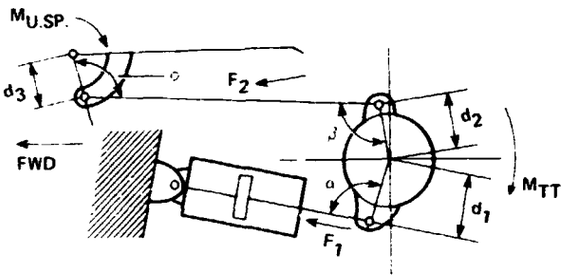

Figure A1.- Upper spoiler control linkage.

Figure A1 shows the relevant features of the upper spoiler control linkage. The forces, angles, and dimensions required to calculate spoiler hinge moment are indicated. Assume zero friction and static loads

$$M_{TT} = M_{SP}$$

$$= F_1 d_1 \sin \alpha$$

$$= F_2 d_2 \sin \beta$$

$$F_2 = F_1 d_1 \frac{\sin \alpha}{d_2 \sin \beta}$$

$$M_{U.SP.} = F_2 d_3 \sin \phi$$

$$= \frac{F_1 d_1 \sin \alpha \, d_3 \sin \phi}{d_2 \sin \beta}$$

$$= \frac{F_1 d_1 d_3}{d_2} \frac{\sin \alpha \sin \phi}{\sin \beta}$$

The angular relationship of the upper spoiler with respect to the various lever angles is shown in figure A2. Now the spoiler hinge moments can be expressed as a function of spoiler position.

$$M_{U.SF.}\Big]_{\delta_{U.SP.}} = \frac{F_1 d_1 d_3}{d_2} \left[\frac{\sin \alpha \sin \phi}{\sin \beta}\right]_{\delta_{U.SP.}} \tag{A1}$$

F_1 = hydraulic pressure (SPPRS) × exposed piston area (A_{eff})

$A_{eff} = A_{pist} - A_{rod} = \frac{\pi}{4} [(3.335^2) - (i.430^2)] = 7.13 \text{ cm}^2 \ (1.105 \text{ in.}^2)$

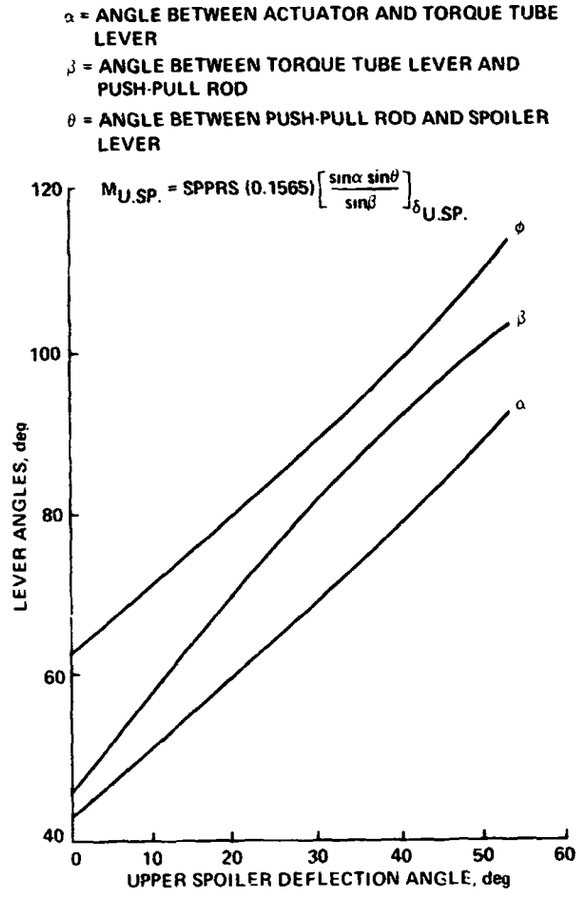

Figure A2.- Upper spoiler lever angles with respect to spoiler angle.

F_1 = 7.13 SPPRS, kg (1.105 SPPRS, lb)

d_1 = 0.0432 m (1.7 in.)

d_2 = 0.0762 m (3.0 in.)

d_3 = 0.0762 m (3.0 in.)

Substituting the above into the moment equation yields the following:

$$M_{U.SP.}\Big]_{\delta_{U.SP.}} = 0.0216\ SPPRS \left[\frac{\sin\alpha \sin\phi}{\sin\beta}\right]_{\delta_{U.SP.}}, \text{ m·kg}$$

$$= 0.15654\ SPPRS \left[\frac{\sin\alpha \sin\phi}{\sin\beta}\right]_{\delta_{U.SP.}}, \text{ ft·lb}$$

The combined multiplying factor for upper spoilers is plotted against spoiler deflection angle in figure 6 of the text.

Lower Spoiler Mechanical and Hydraulic Gearing

Figure A3 shows the essential features of the lower spoiler control linkage, and the information required to calculate spoiler hinge moment are indicated.

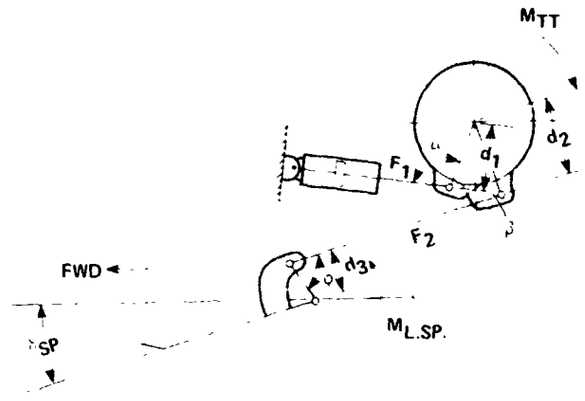

Figure A3.- Lower spoiler control linkage.

Assume zero friction and static loads.

The derivation of lower spoiler hinge moments is identical to the upper spoilers.

$$M_{L.SP.}\Big]_{\delta_{L.SP.}} = \frac{F_1 d_1 d_3}{d_2}\left[\frac{\sin\alpha \sin\ }{\sin\beta}\right]_{\delta_{L.SP.}}$$

The angular relationship of the lower spoiler with respect to the various lever angles is shown in figure A4. This information permits the expression of hinge moments as a function of lower spoiler position.

F_1 is calculated in the same manner as for upper spoilers.

F_1 = 7.13 SPPRS, kg (1.105 SPPRS, lb)

d_1 = 0.0432 m (1.70 in.)

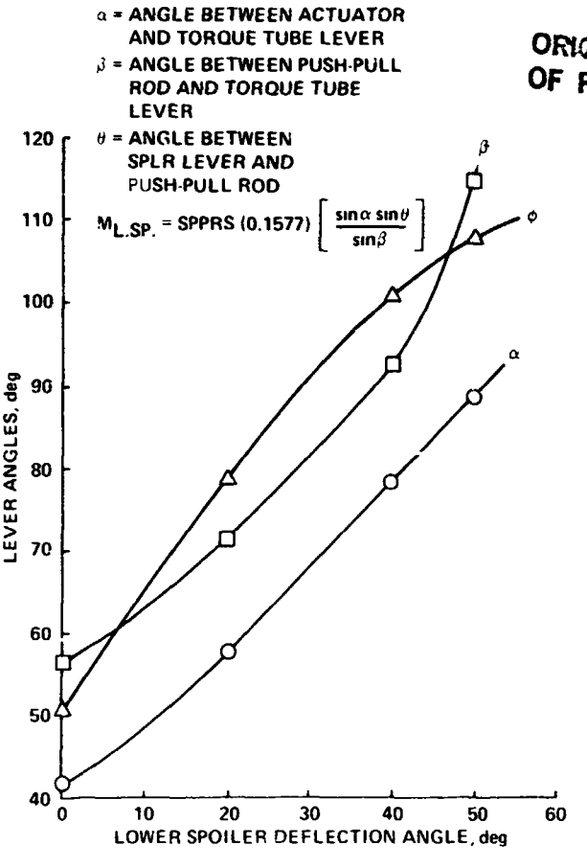

Figure A4.- Lower spoiler lever angles with respect to spoiler angle.

d_2 = 0.0699 m (2.75 in.)

d_3 = 0.0704 m (2.77 in.)

Substituting these values into the moment equation yields the following.

$$M_{L.SP.}\Big]_{\delta_{L.SP.}} = 0.02091 \text{ SPPRS} \left[\frac{\sin\alpha \sin\epsilon}{\sin\beta}\right]_{\delta_{L.SP.}}, \text{ m·kg}$$

$$= 0.15768 \text{ SPPRS} \left[\frac{\sin\alpha \sin\epsilon}{\sin\beta}\right]_{\delta_{L.SP.}}, \text{ ft·lb}$$

The combined multiplying factor for lower spoilers is plotted in figure 6 of the text, with the multiplying factor for upper spoilers.

REFERENCES

1. Beatty, T. D.; Elaschke, A. C.; et al.: Twin Otter Control Modeling. NASA CR 137908, 1976.

2. Olcott, J. W.; Seckel, E.; and Ellis, D. R.: Analysis and Evaluation of a Small, Fixed Wing Aircraft Equipped with Hinged-Plate Spoilers. NASA CR 166247, 1982.

3. Grgurich, J.; and Bradbury, P.: STOLAND Final Report. NASA CR-137972, 1976.

4. Hoerner, Sighard F.: Aerodynamic Drag and Hydrodynamic Resistance. Midland Park, N.J., 1965.

5. Davies, H.; and Kirk, F. N.: A Resume of Aerodynamic Data on Air Brakes. ARC R and M no. 2614, 1951.